

## Photophysical and (Photo)electrochemical Properties of a Coumarin Dye

Zhong-Sheng Wang,<sup>\*,†</sup> Kohjiro Hara,<sup>§</sup> Yasufumi Dan-oh,<sup>||</sup> Chiaki Kasada,<sup>||</sup> Akira Shinpo,<sup>||</sup> Sadaharu Suga,<sup>||</sup> Hironori Arakawa,<sup>†</sup> and Hideki Sugihara<sup>\*,†</sup>

Solar Light Energy Conversion Team, Energy Technology Research Institute, National Institute of Advanced Industrial Science and Technology (AIST), 1-1-1, Higashi, Tsukuba, Ibaraki 305-8565, Japan, Photonics Research Institute, National Institute of Advanced Industrial Science and Technology (AIST), 1-1-1, Higashi, Tsukuba, Ibaraki 305-8565, Japan, and Hayashibara Biochemical Laboratories, Incorporated, 564-176 Fujita, Okayama 701-0221, Japan

Received: November 10, 2004; In Final Form: January 3, 2005

A new coumarin dye, cyano-{5,5-dimethyl-3-[2-(1,1,6,6-tetramethyl-10-oxo-2,3,5,6-tetrahydro-1*H*,4*H*,10*H*-11-oxa-3a-aza-benzo[de]anthracen-9-yl)vinyl]cyclohex-2-enylidene}-acetic acid (NKX-2753), was prepared and characterized with respect to photophysical and electrochemical properties. It was employed as a dye sensitizer in dye-sensitized solar cells and showed efficient photon-to-electron conversion properties. The photocurrent action spectrum exhibited a broad feature with a maximum incident photon-to-electron conversion efficiency (IPCE) of 84% at 540 nm, which is comparable to that for the famous red dye RuL<sub>2</sub>(NCS)<sub>2</sub> (known as N3), where L stands for 2,2'-bipyridyl-4,4'-dicarboxylic acid. The sandwich-type solar cell with NKX-2753, under illumination of full sun (AM1.5, 100 mW cm<sup>-2</sup>), produced 16.1 mA cm<sup>-2</sup> of short-circuit photocurrent, 0.60 V of open-circuit photovoltage, and 0.69 of fill factor, corresponding to 6.7% of overall energy conversion efficiency using 0.1 M LiI, 0.05 M I<sub>2</sub>, 0.1 M guanidinium thiocyanate, and 0.6 M 1,2-dimethyl-3-*n*-propyl-imidazolium iodide in dry acetonitrile as redox electrolyte. In comparison with its analogue NKX-2586 (*Langmuir* 2004, 20, 4205), NKX-2753 with an extra side ring on the alkene chain produced much higher IPCE values at the same conditions. The side ring acted as a spacer to efficiently prevent dye aggregation when adsorbed on the TiO<sub>2</sub> surface, resulting in significant improvements of short-circuit photocurrent, open-circuit photovoltage, and fill factor compared with NKX-2586 that aggregated on the TiO<sub>2</sub> surface.

### Introduction

Dye-sensitized solar cells (DSSCs) have attracted considerable attention since the landmark report by Grätzel's group.<sup>1</sup> In DSSCs, the sensitizer, chemically adsorbed on the TiO<sub>2</sub> surface, absorbs visible light and after excitation injects an electron to the conduction band of TiO<sub>2</sub>, generating electric current. The photovoltage generated by the cell is theoretically the difference between the Fermi level in TiO<sub>2</sub> under illumination and the Nernst potential of the redox couple in the electrolyte.<sup>2</sup> Among the dyestuff tested so far, ruthenium polypyridyl complexes have shown outstanding charge-transfer properties. Overall energy conversion efficiency greater than 10% was achieved with two excellent dyes *cis*-di(thiocyanato)bis(2,2'-bipyridyl-4,4'-dicarboxylate)ruthenium(II) (known as N3)<sup>3</sup> and tri(thiocyanato)-2,2',2''-terpyridyl-4,4',4''-tricarboxylate)ruthenium(II)<sup>4</sup> (known as the black dye). In particular, N3 has been used as the paradigm of a heterogeneous charge-transfer sensitizer in DSSCs. In addition to ruthenium complexes,<sup>3-10</sup> other metal complexes comprising Os<sup>11</sup> and Fe<sup>12</sup> also showed promising results.

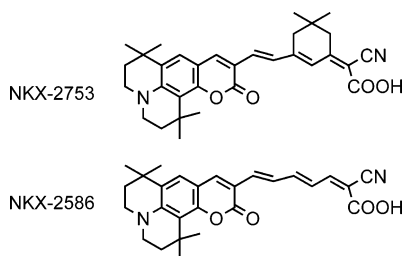
Among the family of dye sensitizers pure organic dyes are also promising due to their rich photophysical properties. Organic dyes have two major advantages in DSSCs. One is the high molar extinction coefficient for the organic dye due to its much higher oscillator strengths than those of metal complexes. The use of organic dyes would allow a thinner TiO<sub>2</sub> film to harvest the incident light efficiently. The other advantage is that no noble metal like Ru is concerned in organic dyes. This reduces the overall cost of the cell production. For these reasons organic dyes may find applications in DSSCs. Recently, several groups reported solar cell performance based on organic dyes, such as cyanines,<sup>13</sup> merocyanines,<sup>14</sup> hemicyanines,<sup>15</sup> perylenes,<sup>16</sup> xanthenes,<sup>17</sup> porphyrins,<sup>18</sup> phthalocyanines,<sup>19</sup> polyenes,<sup>20</sup> polythiophenes,<sup>21</sup> coumarins,<sup>22</sup> etc. Among the organic dyestuff tested so far, coumarin dye may be the most promising sensitizer. Coumarin 343, a laser dye, displayed very high IPCEs in the spectral sensitization of TiO<sub>2</sub> film but produced low photocurrents due to the lack of red and near-IR light absorption.<sup>23</sup> Our group has systematically studied the coumarin dyes and successfully shifted the maximum absorption to the red region by way of expanding  $\pi$ -conjugation through molecular design.<sup>22</sup> As a result of improved photoresponse in the red region, short-circuit photocurrent and overall energy conversion efficiency have been improved significantly. After we obtained an efficiency of 7.7% with a coumarin derivative NKX-2677,<sup>24</sup> Horiuchi et al. achieved an efficiency of 8.00% using an indoline

\* Corresponding authors. E-mail: zs.wang@aist.go.jp, sugihara-hideki@aist.go.jp, Tel: +81-29-861-4643. Fax: +81-29-861-6771.

<sup>†</sup> Energy Technology Research Institute, National Institute of Advanced Industrial Science and Technology (AIST).

<sup>§</sup> Photonics Research Institute, National Institute of Advanced Industrial Science and Technology (AIST).

<sup>||</sup> Hayashibara Biochemical Laboratories, Inc.

**SCHEME 1: Schematic Structure of NKX-2586 and NKX-2753**

dye.<sup>25</sup> These findings indicate that organic dyes are hopefully becoming alternative sensitizers to ruthenium complexes in DSSCs.

One strategy to extend the photoresponse of coumarin to the red region is to introduce methine ( $-\text{CH}=\text{CH}-$ ) units to the coumarin framework with a carboxylic acid ( $-\text{COOH}$ ) group as the anchoring group to  $\text{TiO}_2$  and a cyano ( $-\text{CN}$ ) group as the electron-withdrawing group.<sup>22</sup> Because of the expanded  $\pi$ -conjugation, the lowest energy absorption was shifted to the longer wavelength and the dyes absorb widely in the visible region.<sup>22</sup> Using this strategy we synthesized a series of coumarin derivatives with various numbers of methine units and comparatively studied their photovoltaic properties.<sup>22</sup> It has been found that the maximum absorption was gradually red shifted by increasing the number of methine units from 1 to 3. Although NKX-2586 (Scheme 1), with three methine units, showed the broadest feature of photocurrent action spectrum among the series of dyes tested, IPCE values around the maximum absorption are much lower than those of the other analogues mainly due to dye aggregation.<sup>22</sup> It is well known that dye aggregation is disadvantageous to photocurrent generation because  $\pi$ -stacked aggregation on  $\text{TiO}_2$  may decrease electron injection due to intermolecular energy transfer.<sup>22,26</sup> The strong interaction between NKX-2586 dye molecules on the  $\text{TiO}_2$  surface resulted in aggregation and diminished both photocurrent and photovoltage.<sup>22</sup>

Although coadsorption of NKX-2586 with deoxycholic acid was able to prevent aggregation and hence improve the photovoltaic performance by means of improving both photocurrent and photovoltage,<sup>22</sup> the significantly decreased dye adsorption unavoidably limits the photovoltaic performance. To reduce the intermolecular interaction or dye aggregation and meanwhile keep the adsorbed dye amount, a new dye, NKX-2753 (Scheme 1), was designed and synthesized. When a side ring was introduced to the alkene chain, dye aggregation was prevented efficiently according to the UV-vis absorption and the photocurrent action spectra. In this study we report the photophysical and electrochemical properties of NKX-2753 and the photovoltaic performance of dye-sensitized solar cells. It was found that NKX-2753 is superior to NKX-2586 in terms of cell efficiency because of the prevented dye aggregation.

**Experimental Section**

**Materials and Reagents.** 4-*tert*-Butylpyridine (TBP) and tetrabutylammonium perchlorate (TBAP) were bought from Aldrich and Fluka, respectively. The other reagents used in this study, such as guanidinium thiocyanate (GT), deoxycholic acid (DCA), acetonitrile (AN), etc., were purchased from Wako Pure Chemical Industries Ltd. 1,2-Dimethyl-3-*n*-propylimidazolium iodide (DMPII) was purchased from Tomiyama Pure Chemical Industries Ltd. Transparent conducting oxide (TCO, F-doped  $\text{SnO}_2$ , 10  $\Omega/\square$ ) was provided by Nippon Sheet Glass Co. and

washed with basic solution, ethanol, and acetone successively under supersonication for 10 min each. NKX-2753 was provided by Hayashibara Biochemical Laboratories, and the purity was confirmed by NMR measurement (see Supporting Information). The synthesis of NKX-2586 was reported previously.<sup>22</sup>

**Fabrication of the Dye-Sensitized  $\text{TiO}_2$  Films.** A screen-printing method was used to fabricate  $\text{TiO}_2$  films on TCO glass.  $\text{TiO}_2$  nanoparticles (23 nm) and large particles (100 nm) were prepared by the method reported previously.<sup>27</sup>  $\text{TiO}_2$  nanoparticles (23 nm) and a mixture of nanoparticles (23 nm) and scattering particles (100 nm) at a ratio of 6:4 were dispersed in ethanol. The  $\text{TiO}_2$  pastes were prepared by mixing  $\text{TiO}_2$  suspension, ethyl cellulose, and  $\alpha$ -terpinol in ethanol followed by removal of the solvent ethanol by rotary evaporator at 40  $^\circ\text{C}$  under a vacuum of 20 hPa. Pastes N and M consisted of nanoparticles and mixed particles (23 and 100 nm particles at a ratio of 6:4, respectively). Transparent  $\text{TiO}_2$  films, fabricated on TCO glass using paste N, were used for characterizations such as spectroscopic and electrochemical measurements. Double-layer  $\text{TiO}_2$  films (12  $\mu\text{m}$ ), employed for photovoltaic measurements, were prepared by printing the transparent layer (6  $\mu\text{m}$ ) first with paste N followed by further coating with paste M. The  $\text{TiO}_2$  films were fired at 525  $^\circ\text{C}$  for 2 h with a rising rate of 10  $^\circ\text{C}/\text{min}$ . All the films were immersed in 0.05 M  $\text{TiCl}_4$  solution for 30 min at 70  $^\circ\text{C}$  followed by calcination at 450  $^\circ\text{C}$  for 30 min.<sup>4</sup> The film thickness was measured with a Tencor Alpha-Step 500 Surface Profiler. The film size is apparently 0.5  $\times$  0.5  $\text{cm}^2$ , whose precise area was determined by a digital CCD camera controlled by a computer. The films were immersed in a dye solution for at least 6 h when they were at  $\sim 100$   $^\circ\text{C}$  cooled from the heating. The dye solution (0.3 mM) was prepared in a mixed solvent of AN and 4-*tert*-butyl alcohol with a volume ratio of 1/1.

**Photovoltaic Measurement.** Open (unsealed) and sealed cells were employed for photovoltaic measurements and stability tests, respectively. An open cell was assembled by clipping dye-sensitized  $\text{TiO}_2$  film (working electrode) and Pt-coated TCO glass (counter electrode) together; the two electrodes were separated by a polyethylene spacer. The electrolytes were introduced into the interelectrodes by capillary force. For the sealed cells the two electrodes were separated by a Surlyn spacer (30  $\mu\text{m}$  thick) and sealed up by heating the polymer frame. The redox electrolyte was introduced into the space of interelectrodes through the two holes predrilled on the back of the counter electrode. The two holes were sealed up using a Surlyn film, on which a glass slide was pressed under heat.<sup>27</sup> The redox electrolyte used was 0.1 M LiI, 0.05 M  $\text{I}_2$ , 0.6 M DMPImI, and TBP or GT with various concentrations in dry AN. The current-voltage characteristics of the cells were measured on a PC-controlled source meter (Advantest, R6243) under illumination of simulated AM1.5 solar light from an AM1.5 solar simulator (Wacom Co., Japan, WXS-80C-3 with a 300-W Xe lamp and an AM1.5 filter). The incident light intensity was calibrated with a standard Si solar cell produced by Japan Quality Assurance Organization (JQA). Photocurrent action spectra were recorded on a CEP-99W system (Bunkoh-Keiki Co., Ltd.).

**Characterization.** The UV-vis absorption spectra of the dye-loaded transparent film and the dye solutions were recorded on a Shimadzu UV-3101PC spectrophotometer. The attenuated total reflection Fourier transform infrared (ATR-FTIR) spectra were measured with a Perkin-Elmer Spectrum One spectrometer. Cyclic voltammograms were measured with CH 610B Electrochemical Analyzer. Dye-loaded film, platinum, and  $\text{Ag}/\text{Ag}^+$  (0.01 M  $\text{AgNO}_3$  + 0.1 M TBAP in AN) were employed as

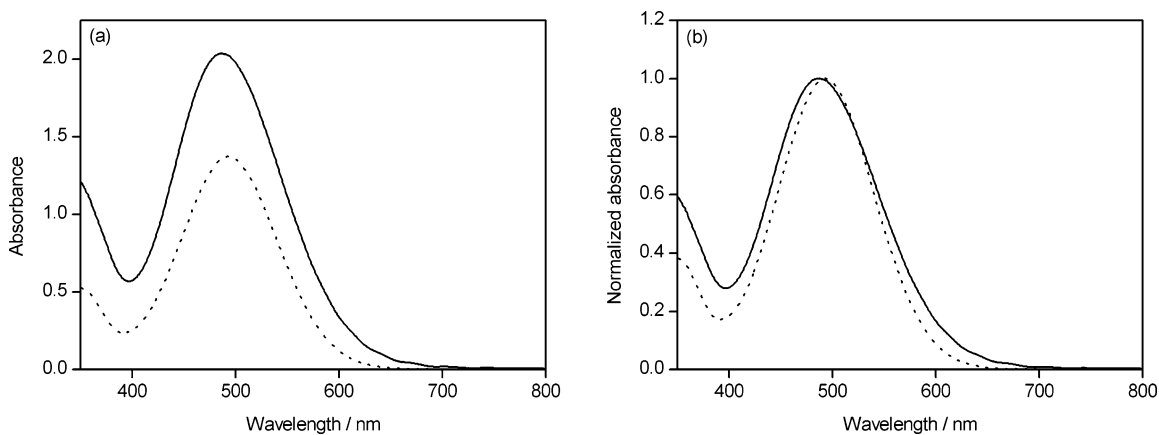


**Figure 1.** (a) UV-vis absorption spectra for  $2.6 \times 10^{-5}$  M NKX-2753 in ethanol (dotted line) and on  $3.5 \mu\text{m}$   $\text{TiO}_2$  transparent film (solid line). Ethanol and  $\text{TiO}_2$ -coated conducting glass were used as references, respectively. (b) Normalized spectra.

working, counter, and reference electrodes, respectively. The supporting electrolyte was 0.1 M TBAP in AN, which was degassed with  $\text{N}_2$  for 20 min prior to scan. The potential of the reference electrode is 0.49 V vs NHE and calibrated with ferrocene.

## Results

**UV-vis Absorption Spectra.** Figure 1a depicts the absorption spectra for NKX-2753 both in ethanol solution and on the  $\text{TiO}_2$  surface. The normalized spectra are shown in Figure 1b. The strong peak at 492 nm is attributed to the  $\pi-\pi^*$  electron transition. The molar extinction coefficient in ethanol was determined to be  $5.03 \times 10^4 \text{ M}^{-1} \text{ cm}^{-1}$  at 492 nm; such a high value is beneficial to light harvesting. After the dye was adsorbed from solution to the surface of  $\text{TiO}_2$ , the absorption spectrum did not show a big difference and the maximum absorption was slightly blue shifted from 492 to 487 nm, as seen in Figure 1b. The 5 nm blue shift was ascribed to the interaction between the dye molecules and  $\text{TiO}_2$ . The absorption threshold at 650 nm for the dye in ethanol is red shifted to 700 nm upon adsorption on the  $\text{TiO}_2$  surface. The interaction between the carboxylate group and the surface  $\text{Ti}^{4+}$  ions may lead to increased delocalization of the  $\pi^*$  orbital of the conjugated framework. The energy of the  $\pi^*$  level is decreased by this delocalization, which explains the red shift for the absorption threshold.<sup>3</sup>

The absorption for NKX-2753 (maximum absorption at 492 nm) is similar to that for NKX-2586 (maximum absorption at 513 nm) in ethanol<sup>22c</sup> due to their similar structure (Scheme 1). However, NKX-2586 exhibited a much bigger blue shift than NKX-2753 after adsorption on  $\text{TiO}_2$ , which will be detailed in the Discussion section.

**FTIR Spectra.** The binding modes of the dye attached to the  $\text{TiO}_2$  surface, which are related to the interfacial electron injection process, were characterized by ATR FTIR.<sup>28</sup> Figure 2 shows FTIR spectra for the free NKX-2753 powder and the dye-loaded  $\text{TiO}_2$  film. For the free dye characteristic bands for cyano ( $\text{C}\equiv\text{N}$ ), carbonyl ( $\text{C}=\text{O}$ ), and carboxylic acid ( $\text{COOH}$ ) were clearly observed at 2204, 1712, and 1666  $\text{cm}^{-1}$ , respectively.<sup>29</sup> After the dye was adsorbed on the  $\text{TiO}_2$  surface, while the IR peaks for cyano and carbonyl groups were also detected at the same frequencies, the 1666  $\text{cm}^{-1}$  peak for carboxylic acid disappeared and instead two new peaks at 1540 and 1371  $\text{cm}^{-1}$ , assignable to the asymmetric and symmetric mode of carboxylate,<sup>29</sup> appeared in the spectrum. This observation indicates deprotonation of the  $\text{COOH}$  group taking place on the  $\text{TiO}_2$  surface. The formed carboxylate ion may coordinate to a metal

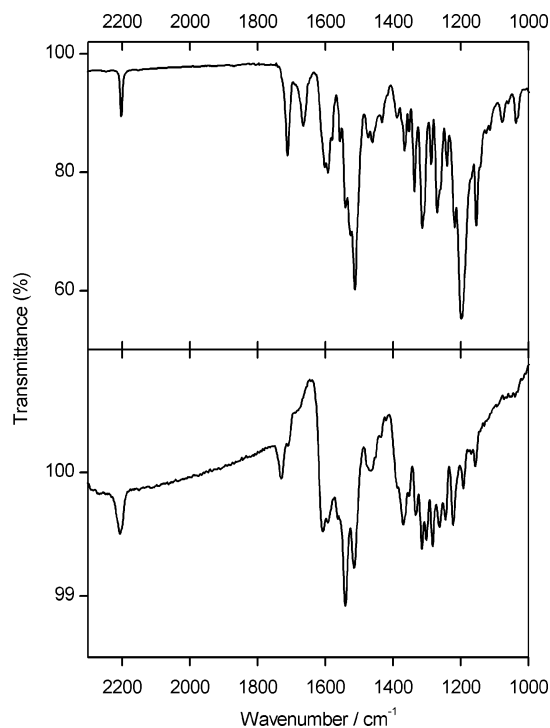
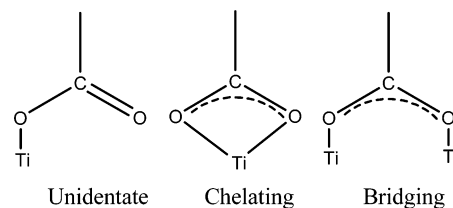


**Figure 2.** ATR-FTIR spectra for NKX-2753 powder (top) and NKX-2753 adsorbed on a  $\text{TiO}_2$  film (bottom).

## SCHEME 2: Possible Binding Modes for Carboxylate Group on $\text{TiO}_2$



ion in several modes (Scheme 2) such as unidentate (i.e., ester), bidentate chelating, bidentate bridging, etc.<sup>30</sup> The frequency separation,  $\Delta\nu = \nu_{\text{as}}(\text{COO}^-) - \nu_{\text{s}}(\text{COO}^-)$ , between asymmetric and symmetric stretching modes of the carboxylate group can be used to determine the binding mode of the dye on the  $\text{TiO}_2$  surface according to an empirical rule proposed by Deacon and Philips.<sup>31</sup> The splitting values are in the order of unidentate > ionic form  $\approx$  bidentate bridging > bidentate chelating.<sup>31</sup> The frequency separations were 242 and 169  $\text{cm}^{-1}$  for the ionic form of the free dye and the dye-loaded film, respectively, suggesting

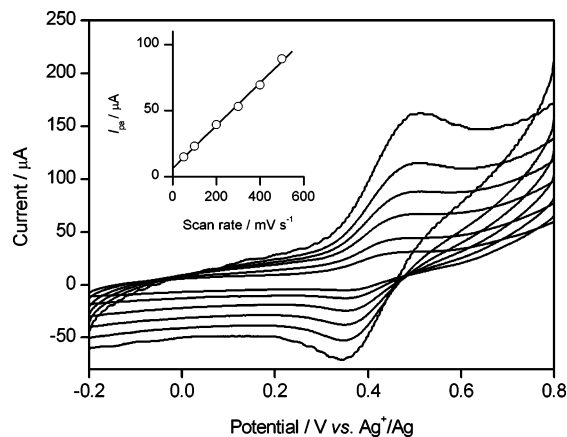


**Figure 3.** Cyclic voltammograms of NKX-2753 adsorbed on 6  $\mu\text{m}$   $\text{TiO}_2$  nanocrystalline film. Scan rates (from inter to outer) are 50, 100, 200, 300, 400, and 500  $\text{mV s}^{-1}$ , respectively. The inset shows the relationship between the anodic peak currents and scan rates.

a bidentate chelating mode for the anchoring of the dye on the  $\text{TiO}_2$  surface. A similar coordination mode for NKX-2586<sup>22c</sup> and a merocyanine dye<sup>14b</sup> was also observed. However, a bidentate bridging mode was suggested for ruthenium complexes adsorbed on  $\text{TiO}_2$ .<sup>32</sup>

**Cyclic Voltammetry (CV).** Figure 3 shows typical cyclic voltammograms of NKX-2753 dye-sensitized 6  $\mu\text{m}$  thick  $\text{TiO}_2$  nanocrystalline film on TCO glass in an AN solution containing 0.1 M TBAP as supporting electrolyte. When the potential was scanned between  $-0.2$  to  $0.8$  V vs  $\text{Ag}^+/\text{Ag}$ , quasi-reversible waves were observed. The formal redox potential,  $(E_{\text{ox}} + E_{\text{red}})/2$ , was calculated to be 0.41 V, corresponding to 0.9 V vs NHE. The anodic and cathodic peak potentials shifted symmetrically, resulting in a constant formal potential at various scan rates. The linear relationship between the anodic peak current and the scan rate, as shown in the inset of Figure 3, indicates a surface-confined electrochemical process.

The formal redox potential is regarded as the highest occupied molecular orbital (HOMO) energy level, and the absorption threshold (700 nm, 1.77 eV) for the dye-loaded  $\text{TiO}_2$  film is roughly taken as the 0–0 transition energy ( $E_{0-0}$ ).<sup>22</sup> Therefore, the lowest unoccupied molecular orbital (LUMO) energy level is deduced to be  $-0.87$  V vs NHE by

$$\text{LUMO} = \text{HOMO} - E_{0-0} \quad (1)$$

The CV for NKX-2586-sensitized  $\text{TiO}_2$  was also measured at the same conditions. The HOMO and LUMO for NKX-2586 were determined to be 0.91 and  $-0.79$  V vs NHE, respectively. It is apparent that the LUMO levels for both dyes are more negative than the conduction band edge of  $\text{TiO}_2$  ( $-0.5$  V vs NHE at pH 7),<sup>2</sup> rendering electron injection thermodynamically possible.

**Photocurrent Action Spectrum.** Incident monochromatic photon-to-electron conversion efficiency (IPCE) is calculated by

$$\text{IPCE}(\lambda) = \frac{1240 \times J_{\text{ph}}[\mu\text{A}/\text{cm}^2]}{\lambda(\text{nm}) \times P[\text{W}/\text{m}^2]} \quad (2)$$

where  $J_{\text{ph}}$  is the photocurrent density generated by monochromatic light with wavelength  $\lambda$  and intensity of  $P$ . IPCE as a function of excitation wavelength is plotted in Figure 4. IPCEs exceed 80% in the range of 450 and 600 nm, attaining a maximum value of 84% at 540 nm. The decrease of the IPCE

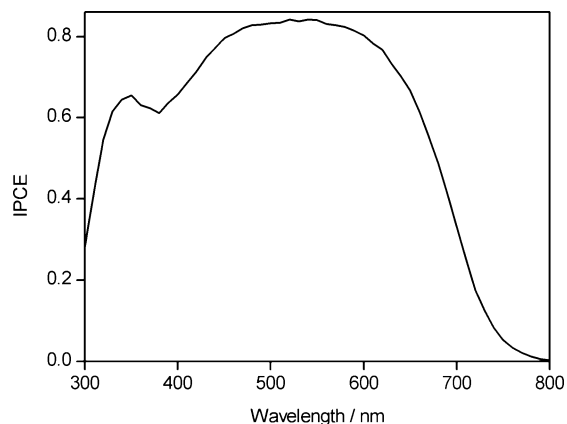


**Figure 4.** IPCE action spectrum for NKX-2753 dye-sensitized solar cell. The electrolyte used was 0.1 M LiI, 0.05 M  $\text{I}_2$ , 0.1 M GT, and 0.6 M DMPImI in dry AN.

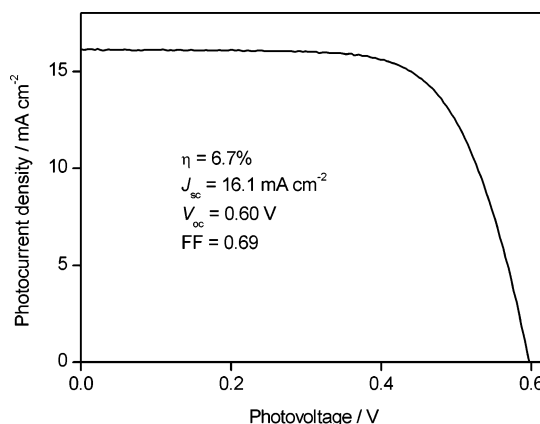


**Figure 5.** Photocurrent–photovoltage characteristics of a NKX-2753 dye-sensitized solar cell under illumination of simulated solar light (AM 1.5, 100  $\text{mW cm}^{-2}$ ). Electrolyte used was the same as that shown in Figure 4.

above 600 nm toward the long-wavelength region stems from the decrease in the extinction coefficient of this dye. On the other hand, the drop of IPCE below 450 nm is mainly ascribed to the filtering of light by the triiodide anions. The peak located at  $\sim 350$  nm in the action spectrum is due to the band gap excitation of  $\text{TiO}_2$  under UV light. Taking the light losses due to light absorption and reflection by the conducting glass and the filtering of light by the electrolyte, IPCEs at wavelengths below 600 nm can be considered to be unity. NKX-2753 showed a broad feature in the action spectrum with IPCE values exceeding 80% below 600 nm. From this point of view, NKX-2753 rivals N3.<sup>3</sup>

**Photovoltaic Performance.** A sandwich-type DSSC composed of NKX-2753 dye-sensitized  $\text{TiO}_2$  film was illuminated under 100  $\text{mW cm}^{-2}$  of simulated AM 1.5 solar light, and the typical current–voltage curve is shown in Figure 5. The electrolyte used is 0.1 M LiI, 0.05 M  $\text{I}_2$ , 0.6 M DMPImI, and 0.1 M GT in dry AN. Like TBP, GT can also improve  $V_{\text{oc}}$  as Grätzel reported.<sup>33</sup> The cell generated 16.1  $\text{mA cm}^{-2}$  of  $J_{\text{sc}}$ , 0.60 V of open-circuit photovoltage ( $V_{\text{oc}}$ ), and 0.69 of fill factor (FF), corresponding to an energy conversion efficiency ( $\eta$ ) of 6.7%. The obtained  $J_{\text{sc}}$  (16.1  $\text{mA cm}^{-2}$ ) almost equals to the integrated photocurrent (16.06  $\text{mA cm}^{-2}$ ) from the action spectrum and the standard global AM1.5 solar emission spectrum. This means the spectral mismatch is very small.

Figure 6 shows the dependence of  $J_{\text{sc}}$  and  $V_{\text{oc}}$  on light intensity for the NKX-2753-based cell.  $J_{\text{sc}}$  increases linearly with light intensity, while  $V_{\text{oc}}$  increases linearly with the

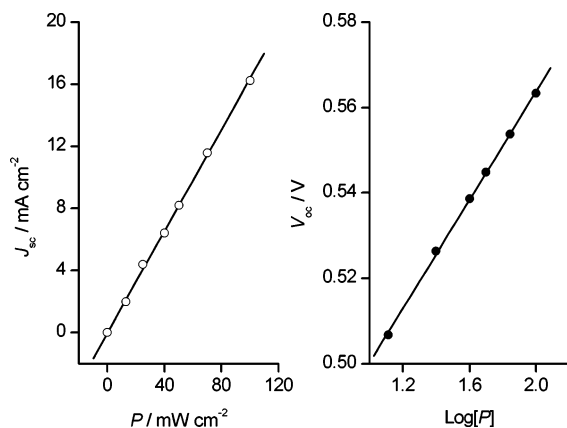


**Figure 6.** (Left) Dependence of short-circuit photocurrent ( $J_{sc}$ ) on the light intensity ( $P$ ). (Right) Dependence of open-circuit photovoltage ( $V_{oc}$ ) on the logarithm of light intensity for NKX-2753-based solar cell.

logarithm of the light intensity. With increasing light intensity, the amount of active dye molecules becomes larger and the transport kinetics of the redox couples plays an important role in the regeneration of dye and hence the photocurrent generation. The linear increase of  $J_{sc}$  with light intensity indicates that the transport of  $I^-/I_3^-$  ions from and to the counter electrode is fast enough to regenerate the dye. It is therefore concluded that photocurrent generation in this system is not limited by the diffusion of the redox species in the electrolyte up to one sun.<sup>3</sup> In liquid-junction DSSCs  $V_{oc}$  is determined by<sup>33b,34</sup>

$$V_{oc} = (nRT/F) \ln[J_{sc}/J_0 - 1] \quad (3)$$

where  $n$  is the ideality factor,  $J_{sc}$  and  $J_0$  are the short-circuit photocurrent and the reverse saturation current, respectively, and  $R$  and  $F$  are the ideal gas and Faraday constants, respectively. If  $J_{sc}$  is much larger than  $J_0$ ,  $V_{oc}$  should be proportional to the logarithm of  $J_{sc}$ , and thus the light intensity because of the linear relationship between the latter two factors. This is the case of the system reflected from the linear dependence of  $V_{oc}$  on the logarithm of light intensity. A similar dependence of  $J_{sc}$  and  $V_{oc}$  on light intensity was also observed for NKX-2586 (not shown).

**Stability.** The poor stability of the organic dye limits its practical applications. Without electrolyte, most of the organic dyes are easy to decompose at the surface of  $TiO_2$  but are stable in the presence of redox species because of the quick regeneration of the dye by the iodide ions. In this study sealed cells with electrolyte of 0.1 M LiI, 0.05 M  $I_2$ , 0.1 M GT, and 0.6 M DMPImI in dry AN were used to conduct stability tests at room temperature. The cells were covered with an L42 cutoff filter ( $\lambda > 420$  nm) and illuminated under simulated AM1.5 solar light ( $100 \text{ mW cm}^{-2}$ ) in the open-circuit mode for 1–2 h each day. After 2 months of operation (about 100 h illumination) the efficiencies were decreased by 5–10%, indicating good stability. The cell stability depends on the nature of the dye, the solvent in the electrolyte, temperature, and the sealing condition. To obtain a stable cell, detailed study on the long-term stability is highly needed.

## Discussion

**Dye Aggregation.** Dyes are known to form aggregation, which is due to the strong coupling between the molecules that causes either a blue shift or a red shift in the absorption band of the aggregate. For a J-type aggregate the absorption band is red shifted relative to the monomer, while a blue shift in the

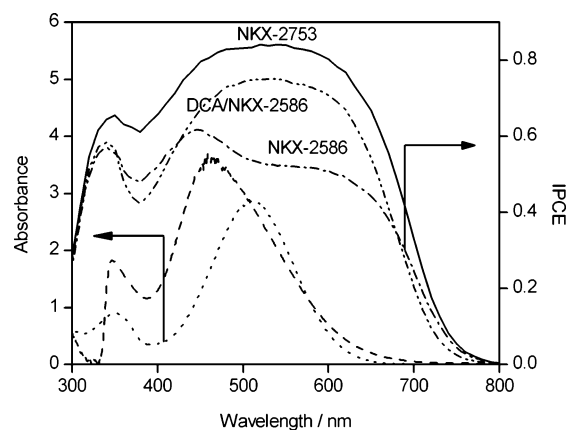


**Figure 7.** UV-vis absorption spectra for NKX-2586 in ethanol ( $\cdots$ ) and on a  $3.5 \mu\text{m}$   $TiO_2$  nanocrystalline film ( $-\cdot-\cdot-$ ), and IPCE action spectra for dye-sensitized  $TiO_2$  film (double layer,  $12 \mu\text{m}$ ) without ( $-\cdot-\cdot-$ ) and with DCA ( $-\cdot-\cdot-$ ). IPCE action spectrum ( $-$ ) for NKX-2753-loaded  $TiO_2$  film (double layer,  $12 \mu\text{m}$ ) is also shown in this figure for convenience of comparison.

absorption band is observed for an H-aggregate.<sup>35</sup> We previously reported the photovoltaic performance of NKX-2586 and found that dye aggregation limited the cell efficiency. Figure 7 shows the UV-vis spectra for NKX-2586 both in solution and on  $TiO_2$  film and IPCE action spectra for NKX-2586 and DCA/NKX-2586. The action spectrum of NKX-2753 is also included in Figure 7 for comparison.

NKX-2586 showed a broad feature in the action spectrum with IPCE values less than 60% as seen in Figure 7. IPCE can be expressed by the product of light harvesting efficiency (LHE), the quantum yield of electron injection ( $\phi_{inj}$ ), and the efficiency of collecting the injected electron ( $\phi_{coll}$ ) at the conducting glass substrate.<sup>3</sup>

$$IPCE(\lambda) = LHE(\lambda) \times \phi_{inj}(\lambda) \times \phi_{coll}(\lambda) \quad (4)$$

If all three factors in eq 4 are unity, the maximum IPCE should fall into the range of 80–85% taking the absorption and reflection by TCO glass into account. Obviously, the maximum IPCE value obtained for NKX-2586 is much lower than the maximum. Since the LHE of NKX-2586-adsorbed film at the maximum absorption, where the absorbance is higher than 5, is unity, either  $\phi_{inj}$  or  $\phi_{coll}$  or both should be less than unity. H-Aggregation usually quenches fluorescence efficiently and would consequently be a loss mechanism competing with electron injection, resulting in lower IPCEs in the visible region.<sup>26</sup> We attribute the lower IPCEs for NKX-2586 to the formation of H-aggregates on the  $TiO_2$  surface, as discussed below.

As we can see from the absorption spectra in Figure 7, the maximum absorption of NKX-2586 was blue shifted by 50 nm from 513 nm in ethanol solution to 463 nm on  $TiO_2$  surface. In addition, the absorption peak became much broader upon adsorption on  $TiO_2$  film from a solution. In agreement with the absorption peak for the dye-loaded film, a peak at 445 nm was observed in the action spectrum. The blue shift by 50 nm of the maximum absorption band, broadening of the absorption spectrum, and low IPCEs generated suggest the formation of H-aggregates when NKX-2586 was adsorbed on the  $TiO_2$  surface. For the dyes tending to aggregate, DCA or the like is usually used as a coadsorbate to prevent aggregation for the purpose of improving cell performance.<sup>4,22,24,36</sup> When 20 mM DCA was included in 0.3 mM NKX-2586, the surface concentration of the dye on  $TiO_2$  was decreased by 70%, but

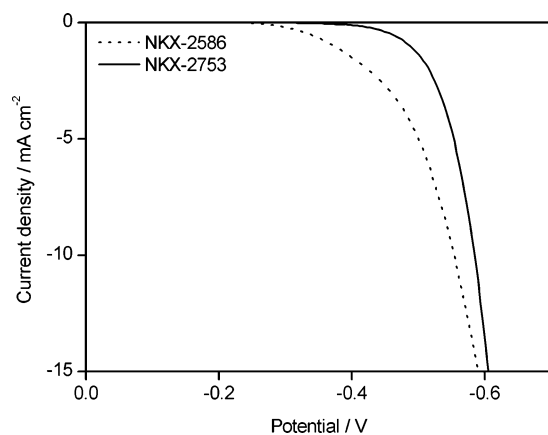


**Figure 8.** Current–potential curves obtained in the dark for NKX-2586 and NKX-2753 dye-sensitized solar cells. The electrolyte used was 0.1 M LiI, 0.05 M I<sub>2</sub>, and 0.6 M DMPImI in AN.

surprisingly the IPCEs between 430 and 680 nm were improved significantly (Figure 7). It is reasonable to attribute this remarkable improvement in IPCE to the prevention of dye aggregation due to DCA.<sup>36</sup> Narrowing of the action spectrum with DCA also supports the formation of aggregation in NKX-2586 because H-aggregation usually broadens the absorption spectrum as compared to the monomer. Although coadsorption of DCA increased IPCE to some extent, the remarkable loss of dye adsorption unavoidably limits the photocurrent generation.<sup>36</sup> To solve this problem NKX-2753 with a side ring, linked to the alkene chain, was designed and prepared (Scheme 1). In contrast to NKX-2586, the UV–vis absorption spectrum of NKX-2753 was not changed much upon adsorption on TiO<sub>2</sub> film from solution (Figure 1). It is concluded from the spectral shifts that NKX-2586 aggregated on the TiO<sub>2</sub> surface whereas NKX-2753 did not. The side ring, acting as a spacer, reduces the coupling between the molecules and therefore prevented aggregation. From this point of view the side ring has a similar function as DCA. However, coadsorption of DCA decreased dye adsorption significantly, while the side ring in the dye did not influence surface concentration of the dye so much. By desorbing the dye into a basic solution we estimated the dye amount by measuring the absorption spectrum of the resultant solution. The surface concentrations were determined to be  $(7.6 \pm 0.2) \times 10^{-8}$  and  $(9.3 \pm 0.2) \times 10^{-8}$  M cm<sup>-2</sup> for NKX-2753 and NKX-2586, respectively. NKX-2753 is bigger than NKX-2586 in molecular size, and therefore, it is reasonable to observe such a difference in the adsorbed amount of dye. Although NKX-2753 has a lower surface concentration on TiO<sub>2</sub> film compared to that of NKX-2586, it generated much higher IPCEs than NKX-2586 in the visible region (Figure 7), which can be explained by the prevention of dye aggregation.

NKX-2753 is superior to NKX-2586 in terms of photovoltaic performance. While NKX-2586 produced an overall efficiency of 3.1% ( $J_{sc} = 13.7$  mA cm<sup>-2</sup>,  $V_{oc} = 0.45$  V, FF = 0.50), NKX-2753 generated an overall efficiency of 5.7% ( $J_{sc} = 16.9$  mA cm<sup>-2</sup>,  $V_{oc} = 0.54$  V, FF = 0.63) using 0.1 M LiI, 0.05 M I<sub>2</sub>, and 0.6 M DMPImI in AN as electrolyte. All three parameters were improved significantly upon introduction of a side ring to the alkene chain, resulting in an increase in efficiency by 84%. Dark current measurement can give a plausible explanation for these observations. The dark current as a function of applied potential is plotted in Figure 8. It is evident that introduction of the side ring suppressed the dark current significantly and shifted the onset potential of dark current from -0.27 to -0.37 V. The 100 mV negative shift is in good agreement with the

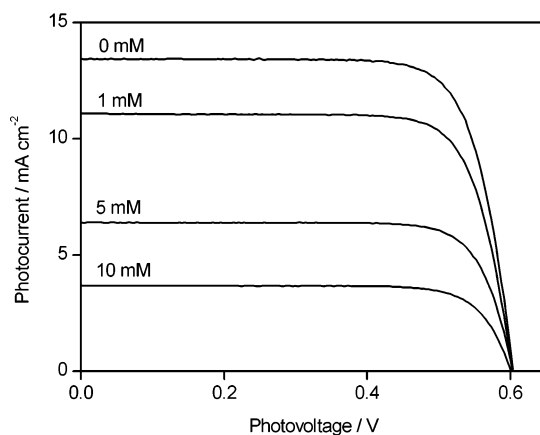


**Figure 9.** Photocurrent–photovoltage characteristics for NKX-2753 dye-sensitized solar cells at various concentrations of DCA in the dye solutions. Electrolyte was 0.1 M LiI, 0.05 M I<sub>2</sub>, 0.2 M TBP, and 0.6 M DMPImI in dry AN.

90 mV increase in  $V_{oc}$ . The dark current represents the reaction between injected electrons and the triiodides. Compared with NKX-2586, the reduced dark current and negative shift of the onset potential for dark current indicate that NKX-2753 favors electron injection and impairs the escape of photoinjected electrons,<sup>37</sup> accounting for the improvements of  $J_{sc}$  and  $V_{oc}$ . This significant improvement of cell performance from NKX-2586 to NKX-2753 supports the prevention of dye aggregation in the latter dye due to the side ring.

Another piece of evidence for the prevention of the aggregation in NKX-2753 comes from the effect of DCA on the photovoltaic performance. As we reported previously, co-grafting of DCA with NKX-2586 improves IPCE and hence  $J_{sc}$  significantly despite the remarkable loss of dye adsorption.<sup>36</sup> The mixed DCA/NKX-2586 seems better than the dye alone in terms of cell efficiency, which was explained by the observation of reduced dark current and negative shift of dark current onset due to the coadsorbate.<sup>36</sup> Contrasting to NKX-2586, DCA gave a different effect on the performance of NKX-2753. Figure 9 shows the effect of DCA on  $I$ – $V$  curves of NKX-2753. With increasing the concentration of DCA,  $J_{sc}$  decreased dramatically while  $V_{oc}$  remained almost same. This behavior is quite different from that of NKX-2586, where suppression of charge recombination due to DCA overrides the significant loss of dye adsorption, resulting in increased  $J_{sc}$  and  $V_{oc}$ .<sup>36</sup> Compared with NKX-2586, DCA had a larger influence on adsorption of NKX-2753 on the TiO<sub>2</sub> surface. At 20 mM DCA, the surface concentration of NKX-2586 was decreased by about 70% whereas NKX-2753 was not adsorbed on the TiO<sub>2</sub> surface. This suggests that NKX-2753 has a weaker interaction than NKX-2586 between molecules, consistent with the spectral shifts (Figures 1 and 7). The presence of DCA with NKX-2753 did not influence the dark current noticeably, resulting in a similar  $V_{oc}$ . The decreased  $J_{sc}$  was ascribed to the decreased dye adsorption. Unlike NKX-2586, DCA is not needed for NKX-2753 to improve cell performance. This means that charge recombination in NKX-2753 is much less significant than that in NKX-2586. Interestingly, the increase in  $V_{oc}$  of 90 mV induced by coadsorption of DCA<sup>36</sup> is equal to that by the side ring. This suggests that the side ring has a similar effect on  $V_{oc}$  as DCA.

Of course, there are many other factors, such as HOMO and LUMO energy levels, influencing photocurrent generation.<sup>38</sup> Assuming that 0.2 eV of the energy difference between the LUMO of the dye and the conduction band edge of TiO<sub>2</sub> is

**TABLE 1: Effect of TBP on the Cell Performance for NKX-2753<sup>a</sup>**

c (TBP)/M	$J_{sc}/\text{mA cm}^{-2}$	$V_{oc}/\text{V}$	FF	$\eta$ (%)
0	16.9	0.54	0.63	5.7
0.1	14.6	0.61	0.70	6.2
0.2	14.1	0.62	0.74	6.5
0.3	12.5	0.64	0.73	5.9
0.4	11.2	0.66	0.74	5.5
0.5	10.3	0.68	0.75	5.3

<sup>a</sup> The cell was illuminated under  $100 \text{ mW cm}^{-2}$  of simulated AM1.5 solar light. The electrolyte used was 0.1 M LiI, 0.05 M  $\text{I}_2$ , 0.6 M DMPImI, and TBP in dry AN.

**TABLE 2: Effect of GT on the Cell Performance for NKX-2753<sup>a</sup>**

c(GT)/M	$J_{sc}/\text{mA cm}^{-2}$	$V_{oc}/\text{V}$	FF	$\eta$ (%)
0	16.9	0.54	0.63	5.7
0.01	16.0	0.57	0.66	6.0
0.05	15.7	0.58	0.70	6.4
0.1	15.5	0.62	0.70	6.7
0.3	13.6	0.63	0.70	6.0
0.5	13.4	0.65	0.70	6.1

<sup>a</sup> The cell was illuminated under  $100 \text{ mW cm}^{-2}$  of simulated AM1.5 solar light. The electrolyte used was 0.1 M LiI, 0.05 M  $\text{I}_2$ , 0.6 M DMPImI, and GT in dry AN.

necessary for efficient electron injection,<sup>38</sup> the driving force for electron injection of NKX-2753 and NKX-2586 should be similar. On the basis of the spectral shifts, IPCE values, and energy levels we analyzed the side ring in NKX-2753 acted as a spacer to prevent dye aggregation, leading to remarkable improvement in device performance compared with NKX-2586.

**Effect of TBP and GT.** Treating the dye-sensitized  $\text{TiO}_2$  electrode with TBP significantly improves both  $V_{oc}$  and the energy conversion efficiency for N3.<sup>3</sup> Frank and co-workers studied the effect of TBP on charge recombination in DSSCs based on N3. TBP was found to lower the rate constant for triiodide reduction by 1–2 orders of magnitude.<sup>34</sup> The suppressed charge recombination between injected electrons and triiodide ions and the negative movement of conduction band edge due to TBP are responsible for the improved  $V_{oc}$ .<sup>34</sup> TBP is also effective in improving the  $V_{oc}$  of some organic dyes.<sup>22,24,36</sup> For example, 1 M TBP increases  $V_{oc}$  from 0.47 to 0.73 V and the overall efficiency from 3.6% to 7.7% for NKX-2677.<sup>35</sup> Contrasting to NKX-2677, NKX-2753 is less sensitive to TBP. The effect of TBP content in the electrolyte on cell performance is summarized in Table 1. With increasing TBP,  $J_{sc}$  decreased,  $V_{oc}$  increased, and FF increased until 0.2 M and then remained almost unchanged. The best efficiency was obtained at 0.2 M TBP for NKX-2753. Without TBP, NKX-2677, one of the best organic dye sensitizers, only generated an efficiency of 3.6% but NKX-2753 produced an efficiency of 5.7%, which is comparable to N3 with an efficiency of 5.8% at similar conditions.<sup>34</sup> As TBP is able to desorb the dye from the  $\text{TiO}_2$  surface, it is very important to get high efficiency at low TBP content or without TBP for the benefit of long-term stability.

GT as additive was first reported by Grätzel.<sup>33</sup> Coadsorption of GT with N719 results in a remarkable improvement in  $V_{oc}$  due to a reduction in dark current.<sup>33</sup> A new record efficiency of 11% was achieved recently with this approach.<sup>33b</sup> We also checked the effect of GT on the cell performance for NKX-2753 and list the results in Table 2. With increasing GT concentration,  $J_{sc}$  decreased,  $V_{oc}$  increased, and FF increased until 0.05 M GT. Consequently, the maximum energy conversion efficiency (6.7%) was reached at 0.1 M GT. A similar trend

of the GT effect on NKX-2586 was observed. Like NKX-2753, the best efficiency for NKX-2586 (5.4%) was obtained at 0.1 M GT too.

The GT effect is similar to the TBP effect. However, the increase in  $V_{oc}$  by GT (Table 2) is less remarkable than that by TBP (Table 1), while the decrease in  $J_{sc}$  by TBP is larger than that by GT. As a consequence, GT treatment gave a little higher efficiency than TBP treatment.

## Conclusions

To prevent dye aggregation of NKX-2586 and hence improve the cell efficiency, a new coumarin dye with a side ring, NKX-2753, was designed and synthesized. The side ring linked to the alkene chain was proved to be effective to prevent dye aggregation as DCA. For this reason, DCA is not needed to coadsorb with NKX-2753 on the  $\text{TiO}_2$  surface, ensuring a high surface concentration of dye and efficient photon-to-electron conversion. From NKX-2586 to NKX-2753 the extra side ring resulted in a remarkable improvement in  $J_{sc}$ ,  $V_{oc}$ , and FF. This finding may be useful to design and synthesize new efficient dye sensitizers in DSSCs. In particular, the cell based on NKX-2753 generated an efficiency of 5.7% in the absence of additive such as TBP and GT; such a high value is very important for long-term stability.

**Acknowledgment.** This work was supported by the New Energy and Industrial Technology Development Organization (NEDO) under the Ministry of Economy of Japan.

**Supporting Information Available:** Synthesis procedure and NMR data for NKX-2753. This material is available free of charge via the Internet at <http://pubs.acs.org>.

## References and Notes

- (1) O'Regan, B.; Grätzel, M. *Nature* **1991**, *353*, 737.
- (2) Hagfeldt, A.; Grätzel, M. *Chem. Rev.* **1995**, *95*, 49.
- (3) Nazeeruddin, M. K.; Kay, A.; Rodicio, I.; Humphry-Baker, R.; Müller, E.; Liska, P.; Vlachopoulos, N.; Grätzel, M. *J. Am. Chem. Soc.* **1993**, *115*, 6382.
- (4) Nazeeruddin, M. K.; Péchy, P.; Renouard, T.; Zakeeruddin, S. M.; Humphry-Baker, R.; Comte, P.; Liska, P.; Cevey, L.; Costa, E.; Shklover, V.; Spiccia, L.; Deacon, G. B.; Bignozzi, C. A.; Grätzel, M. *J. Am. Chem. Soc.* **2001**, *123*, 1613.
- (5) (a) Yanagida, M.; Islam, A.; Tachibana, Y.; Fujihashi, G.; Katoh, R.; Sujihara, H.; Arakawa, H. *New J. Chem.* **2002**, *26*, 963. (b) Islam, A.; Sujihara, H.; Yanagida, M.; Hara, K.; Fujihashi, G.; Tachibana, Y.; Katoh, R.; Murata, S.; Arakawa, H. *New J. Chem.* **2002**, *26*, 966. (c) Hara, K.; Sujihara, H.; Tachibana, Y.; Islam, A.; Yanagida, M.; Sayama, K.; Arakawa, H. *Langmuir* **2001**, *17*, 5992.
- (6) (a) Wang, Z.-S.; Huang, C.-H.; Zhang, B.-W.; Hou, Y.-J.; Xie, P.-H.; Qian, H.-J.; Ibrahim, K. *New J. Chem.* **2000**, *24*, 567. (b) Wang, Z.-S.; Huang, C.-H.; Huang, Y.-Y.; Zhang, B.-W.; Xie, P.-H.; Hou, Y.-J.; Ibrahim, K.; Qian, H.-J.; Liu, F.-Q. *Sol. Energy Mater. Sol. Cells* **2002**, *71*, 261.
- (7) (a) Amadelli, R.; Argazzi, R.; Bignozzi, C. A.; Scandola, F. *J. Am. Chem. Soc.* **1990**, *112*, 7099. (b) Argazzi, R.; Bignozzi, C. A.; Yang, M.; Hasselmann, G. M.; Meyer, G. J. *Nano Lett.* **2002**, *2*, 625.
- (8) (a) Wang, P.; Zakeeruddin, S. M.; Moser, J. E.; Nazeeruddin, M. K.; Sekiguchi, T.; Grätzel, M. *Nat. Mater.* **2003**, *2*, 402. (b) Renouard, T.; Fallahpour, R.-A.; Nazeeruddin, M. K.; Humphry-Baker, R.; Gorelsky, S. I.; Lever, A. B. P.; Grätzel, M. *Inorg. Chem.* **2002**, *41*, 367.
- (9) Hou, Y.-J.; Xie, P.-H.; Zhang, B.-W.; Cao, Y.; Xiao, X.-R.; Wang, W.-B. *Inorg. Chem.* **1999**, *38*, 6320.
- (10) Kilsa, K.; Mayo, E. I.; Kuciauskas, D.; Villahermosa, R.; Lewis, N. S.; Winkler, J. R.; Gray, H. B. *J. Phys. Chem. A* **2003**, *107*, 3397.
- (11) Sauve, G.; Cass, M. E.; Doig, S. J.; Lauermann, I.; Pomykal, K.; Lewis, N. S. *J. Phys. Chem. B* **2000**, *104*, 3488.
- (12) Ferrere, S.; Gregg, B. A. *J. Am. Chem. Soc.* **1998**, *120*, 843.
- (13) (a) Sayama, K.; Tsukugoshi, S.; Mori, T.; Hara, K.; Ohga, Y.; Shinpou, A.; Abe, Y.; Suga, S.; Arakawa, H. *Sol. Energy Mater. Sol. Cells* **2003**, *80*, 47. (b) Ehret, A.; Stuhl, L.; Spittler, M. T. *J. Phys. Chem. B* **2001**, *105*, 9960.
- (14) (a) Sayama, K.; Hara, K.; Tsukugoshi, S.; Abe, Y.; Mori, T.; Satsuki, M.; Suga, S.; Sugihara, H.; Arakawa, H. *Chem. Commun.* **2000**,

1173. (b) Sayama, K.; Shingo, T.; Hara, K.; Ohga, Y.; Shinpo, A.; Abe, Y.; Suga, S.; Arakawa, H. *J. Phys. Chem. B* **2002**, *106*, 1363.
- (15) (a) Wang, Z.-S.; Li, F.-Y.; Huang, C.-H.; Wang, L.; Wei, M.; Jin, L.-P.; Li, N.-Q. *J. Phys. Chem. B* **2000**, *104*, 9676. (b) Wang, Z.-S.; Li, F.-Y.; Huang, C.-H. *Chem. Commun.* **2000**, 2063. (c) Wang, Z.-S.; Li, F.-Y.; Huang, C.-H. *J. Phys. Chem. B* **2001**, *105*, 9210. (d) Wang, Z.-S.; Huang, Y.-Y.; Huang, C.-H.; Zheng, J.; Cheng, H.-M.; Tian, S.-J. *Synth. Met.* **2000**, *114*, 201. (e) Yao, Q.-H.; Meng, F.-S.; Li, F.-Y.; Tian, H.; Huang, C.-H. *J. Mater. Chem.* **2003**, *13*, 1048.
- (16) (a) Ferrere, S.; Zaban, A.; Gregg, B. A. *J. Phys. Chem. B* **1997**, *101*, 4490. (b) Ferrere, S.; Gregg, B. A. *New J. Chem.* **2002**, *26*, 1155. (c) Wang, Z.-S.; Huang, C.-H.; Li, F.-Y.; Weng, S.-F.; Ibrahim, K.; Liu, F.-Q. *J. Phys. Chem. B* **2001**, *105*, 4230. (d) Wang, Z.-S.; Huang, C.-H.; Li, F.-Y.; Weng, S.-F.; Yang, S.-M. *J. Photochem Photobiol. A* **2001**, *140*, 255. (e) Wang, Z.-S.; Huang, C.-H.; Li, F.-Y.; Yang, S.-M.; Weng, S.-F.; Fu, X.-Y.; Wu, N.-Z.; Ibrahim, K.; Liu, F.-Q.; Qian, H.-J. *Sci. China, Ser. B* **2001**, *44*, 268.
- (17) (a) Gerischer, H.; Tributsch, H. *Ber. Bunsen-Ges. Phys. Chem.* **1968**, *72*, 437. (b) Tsubomura, H.; Matsumura, M.; Nomura, Y.; Amamiya, T.; *Nature* **1976**, *261*, 402. (c) Sayama, K.; Sugino, M.; Sugihara, H.; Abe, Y.; Arakawa, H. *Chem. Lett.* **1998**, 753.
- (18) (a) Jasieniak, J.; Johnston, M.; Waclawik, E. R. *J. Phys. Chem. B* **2004**, *108*, 12962. (b) Watson, D. F.; Marton, A.; Stux, A. M.; Meyer, G. *J. Phys. Chem. B* **2004**, *108*, 11680. (c) Kroeze, J. E.; Savenije, T. J.; Warman, J. M. *J. Am. Chem. Soc.* **2004**, *126*, 7608.
- (19) (a) He, J.; Benko, G.; Korodi, F.; Polivka, T.; Lomoth, R.; Akermark, B.; Sun, L.; Hagfeldt, A. *J. Am. Chem. Soc.* **2002**, *124*, 4922. (b) Amao, Y.; Komori, T. *Langmuir* **2003**, *19*, 8872. (c) Huisman, C. L.; Goossens, A.; Schoonman, J. *J. Phys. Chem. B* **2002**, *106*, 10578.
- (20) (a) Hara, K.; Kurashige, M.; Ito, S.; Shinpo, A.; Suga, S.; Sayama, K.; Arakawa, H. *Chem. Commun.* **2003**, 252. (b) Kitamura, T.; Ikeda, M.; Shigaki, K.; Inoue, T.; Anderson, N. A.; Ai, X.; Lian, T.; Yangagida, S. *Chem. Mater.* **2004**, *16*, 1806.
- (21) (a) Senadeera, G. K. R.; Nakamura, K.; Kitamura, T.; Wada, Y.; Yanagida, S. *Appl. Phys. Lett.* **2003**, *83*, 5470. (b) Kim, Y.-G.; Walker, J.; Samuelson, L. A.; Kumar, J. *Nano Lett.* **2003**, *3*, 523.
- (22) (a) Hara, K.; Sayama, K.; Ohga, Y.; Shinpo, A.; Suga, S.; Arakawa, H. *Chem. Commun.* **2001**, 569. (b) Hara, K.; Tachibana, Y.; Ohga, Y.; Shinpo, A.; Suga, S.; Sayama, K.; Sugihara, H.; Arakawa, H. *Sol. Energy Mater. Sol. Cells* **2003**, *77*, 89. (c) Hara, K.; Sato, T.; Katoh, R.; Furube, A.; Ohga, Y.; Shinpo, A.; Suga, S.; Sayama, K.; Sugihara, H.; Arakawa, H. *J. Phys. Chem. B* **2003**, *107*, 597.
- (23) Enea, O.; Moser, J.; Grätzel, M. *J. Electroanal. Chem.* **1989**, 259, 59.
- (24) Hara, K.; Kurashige, M.; Dan-oh, Y.; Kasada, C.; Shinpo, A.; Suga, S.; Sayama, K.; Arakawa, H. *New J. Chem.* **2003**, *27*, 783.
- (25) Horiuchi, T.; Miura, H.; Sumioka, K.; Uchida, S. *J. Am. Chem. Soc.* **2004**, *126*, 12218.
- (26) Khazraji, A. C.; Hotchandani, S.; Das, S.; Kamat, P. V. *J. Phys. Chem. B* **1999**, *103*, 4693.
- (27) Wang, Z. S.; Kawauchi, H.; Kashima, T.; Arakawa, H. *Coord. Chem. Rev.* **2004**, *248*, 1381.
- (28) Argazzi, R.; Binozzi, C. A.; Heimer, T. A.; Castellano, F. N.; Meyer, G. *J. Inorg. Chem.* **1994**, *33*, 5741.
- (29) Socrates, G. *Infrared Characteristic Group Frequencies*, 2nd ed.; Wiley & Sons Ltd.: Baffins Lane, Chichester, England, 1994.
- (30) Shklover, V.; Ovchinnikov, Y. E.; Braginsky, L. S.; Zakeeruddin, S. M.; Grätzel, M. *Chem. Mater.* **1998**, *10*, 2533.
- (31) Deacon, G. B.; Phillips, R. J. *Coord. Chem. Rev.* **1980**, *33*, 227.
- (32) (a) Finnie, K. S.; Bartlett, J. R.; Woolfrey, J. L. *Langmuir* **1998**, *14*, 2744. (b) Duffy, N. W.; Dobson, K. D.; Gordon, K. C.; Robinson, B. H.; Quillan, A. J. M. *Chem. Phys. Lett.* **1997**, *266*, 451. (c) Klein, C.; Nazeeruddin, M. K.; Censo, D. D.; Liska, P.; Grätzel, M. *Inorg. Chem.* **2004**, *43*, 4216. (d) Bauer, C.; Boschloo, G.; Mukhtar, E.; Hagfeldt, A. *J. Phys. Chem. B* **2002**, *106*, 12693.
- (33) (a) Grätzel, M. *J. Photochem. Photobiol. C* **2003**, *4*, 145. (b) Grätzel, M. *J. Photochem. Photobiol. A* **2004**, *164*, 3.
- (34) Huang, S. Y.; Schlichthörl, G.; Nozik, A. J.; Grätzel, M.; Frank, A. J. *J. Phys. Chem. B* **1997**, *101*, 2576.
- (35) (a) McRae, E. G.; Kasha, M. *J. Chem. Phys.* **1958**, *28*, 721. (b) Kasha, M.; Rawls, H. R.; El-Bayoumi, M. A. *Pure Appl. Chem.* **1965**, *11*, 371.
- (36) Hara, K.; Dan-oh, Y.; Kasada, C.; Ohga, Y.; Shinpo, A.; Suga, S.; Sayama, K.; Arakawa, H. *Langmuir* **2004**, *20*, 4205.
- (37) Wang, P.; Zakeeruddin, S. M.; Comte, P.; Charvet, R.; Humphry-Baker, R.; Grätzel, M. *J. Phys. Chem. B* **2003**, *107*, 14336.
- (38) Katoh, R.; Furube, A.; Yoshihara, T.; Hara, K.; Fujihashi, G.; Takano, S.; Murata, S.; Arakawa, H.; Tachiya, M. *J. Phys. Chem. B* **2004**, *108*, 4818.